Quantum versus classical nature of the low-temperature magnetic phase transition in TbAl$_3$(BO$_3$)$_4$

T. Zajarniuk [1], A. Szewczyk [1,*] P. Wiśniewski [2], M. U. Gutowska [1], R. Puzniak [1], H. Szymczak [1], I. Gudim [3],
V. A. Bedarev [4], M. I. Pashchenko [4,5], P. Tomczak [6], and W. Szuszkiewicz [1]

[1]*Institute of Physics, Polish Academy of Sciences, Aleja Lotników 32/46, PL-02668 Warsaw, Poland*

[2]*Institute of Low Temperature and Structure Research, Polish Academy of Sciences, ulica Okólna 2, PL-50422 Wrocław, Poland*

[3]*Kirensky Institute of Physics, Federal Research Center KSC SB RAS, Krasnoyarsk 660036, Russia*

[4]*B. Verkin Institute for Low Temperature Physics and Engineering of the National Academy of Sciences of Ukraine,
47 Nauky Avenue, UA-61103 Kharkiv, Ukraine*

[5]*Institute of Physics, Czech Academy of Sciences, Cukrovarnická 10, 162 00 Praha 6, Czech Republic*

[6]*Faculty of Physics, Adam Mickiewicz University, Uniwersytetu Poznańskiego 2, PL-61614 Poznań, Poland*

Specific heat C_B of a TbAl$_3$(BO$_3$)$_4$ crystal was studied for 50 mK $< T <$ 300 K with emphasis on $T <$ 1 K where a phase transition was found at $T_c = 0.68$ K. Nuclear, nonphonon (C_m), and lattice contributions to C_B were separated. Lowering of T_c with an increase in magnetic field parallel to the easy magnetization axis ($B_\parallel$) was found. It was established that C_m and a Grüneisen ratio depend on $B_\parallel$ and T in a way characteristic of systems in which a classical transition is driven by quantum fluctuations (QFs) to a quantum critical point at $T = 0$ by tuning a control parameter ($B_\parallel$). The $B_\parallel - T$ phase diagram was constructed, and the dynamical critical exponent $0.82 \leqslant z \leqslant 0.96$ was assessed. Nature of the transition was not established explicitly. Magnetization studies point at the ferromagnetic ordering of Tb^{3+} magnetic moments, however, lowering of T_c with increase in $B_\parallel$ is opposite to the classical behavior. Hence, a dominant role of QFs was supposed.

I. INTRODUCTION

Quantum phase transitions (QPTs) induced at zero-temperature T by quantum fluctuations (QFs) as the result of tuning a certain control parameter, e.g., pressure or magnetic field B, are a topical subject of research in condensed-matter physics [1]. As the phenomena appearing at inaccessible experimentally $T = 0$, they are much more difficult for investigation than the classical phase transitions, induced by thermal fluctuations. Their existence can be recognized only by investigating certain unusual properties induced by them at finite T near the quantum critical point (QCP). For example, near QCP, unconventional superconductivity and pronounced non-Fermi-liquid effects in metallic systems were observed [2]. Moreover, at the classical transitions, some thermodynamic quantities being the second derivatives of the thermodynamic potential diverge, whereas due to the third law of thermodynamics, some of these divergences, e.g., of specific heat, disappear at QCP. According to Refs. [3,4], in such a case, the parameter Γ,

$$\Gamma = -\frac{1}{T}\frac{(\partial S/\partial B)_T}{(\partial S/\partial T)_B} = -\frac{(\partial M/\partial T)_B}{C_B(T)} = \frac{1}{T}\left(\frac{\partial T}{\partial B}\right)_S \quad (1)$$

called the magnetic Grüneisen ratio is much more informative because it should diverge and change sign at QCP. Γ is proportional to the ratio of the sensitivity of entropy S to the control parameter B (i.e., $\partial S/\partial B$), growing near QPT, to the sensitivity of S to T (i.e., $\partial S/\partial T$), growing near the classical transition. By using standard thermodynamic transformations and the Maxwell relation, it can be shown (1) that Γ is the ratio of the measurable quantities, i.e., of the minus derivative of magnetization M with respect to T at fixed B to the specific heat C_B or the (multiplied by $1/T$) adiabatic change in T under the influence of B. The latter value is the main parameter characterizing magnetocaloric effect.

Whereas many papers considered QPTs in metallic, heavy-fermion, and/or superconducting systems [2], experimental papers on QPTs in insulating anti- or ferromagnets are scarce and, in majority, consider pyrochlores [5] or organic systems in which magnetic moments arranged in chains or planes are considered by using the Ising or Heisenberg models, e.g., Refs. [6–8]. Whereas the quantum Ising system located in B perpendicular to the Ising axis is the basic and intuitively clear example of the system showing QPT, the bulk TbAl$_3$(BO$_3$)$_4$ crystal seems to be a unique ferromagnetic Ising system in which the temperature of the magnetic transition, discovered by us below 1 K and reported initially in Ref. [9], is lowered and driven to (as we suppose) QCP by B applied along the Ising axis. This is a counterintuitive behavior because in "normal" ferromagnets, B applied along the easy axis supports the low-temperature phase and lifts the transition temperature. Our paper is aimed: (i) at presenting measurements of C_B and M of the TbAl$_3$(BO$_3$)$_4$ single crystal, demonstrating the presence and evolution of the magnetic transition under influence of B, (ii) at analyzing whether near the transition point, the specific heat, magnetization, and Γ-parameter behaviors as functions of T and $B_\parallel$ are consistent with universal behaviors,
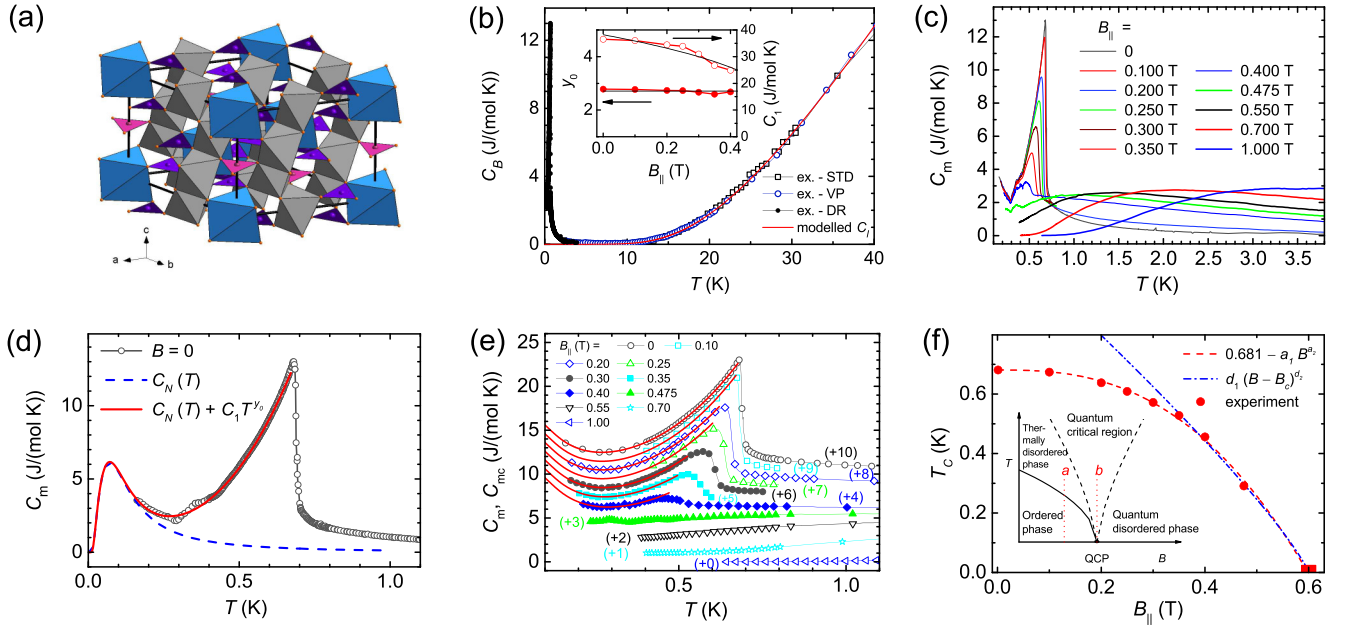
*szewc@ifpan.edu.pl

FIG. 1. Specific heat of the $TbAl_3(BO_3)_4$ single crystal. (a) Trigonal structure of $TbAl_3(BO_3)_4$ with lattice parameters $a = 9.2926(9)$ and $c = 7.2516(4)$ Å. Magnetic Tb^{3+} ions are located inside the deformed (blue) trigonal prisms, located along the threefold c axis, and formed by six O^{2-} ions. (b) Total specific heat C_B measured in $B = 0$ with a standard calorimeter (STD), vertical puck (VP), and dilution refrigerator (DR). The red solid line presents the estimated C_l. In the inset, C_1 and y_0 coefficients of the curves defined by Eq. (5) and fitted to the experimental data shown in the panel (e) are presented as a function of $B_\parallel$. (c) Nonphonon contribution C_m to C_B for several $B_\parallel$ values. (d) Experimental $C_m(T, B = 0)$ function (circles), estimated nuclear specific heat C_N (blue dashed line), and fit of the $C_N(T) + C_1 T^{y_0}$ function to $C_m(T, B = 0)$ (red solid line). Near 330 mK a sinusoidal apparatus effect is visible. (e) Determined $C_{mc}(T)$ (i.e., $C_m(T)$ corrected for the apparatus effect for $B_\parallel \leqslant 0.475$ T and $C_m(T)$ for $B_\parallel > 0.475$ T), symbols, and $C_m(T) = C_N(T) + C_1 T^{y_0}$ functions fitted to these curves (red solid lines). To maintain readability, the curves for different $B_\parallel$ values are shifted along the vertical axis by the values given in parentheses. (f) $B_\parallel - T$ phase diagram found based on $C_m(T, B_\parallel)$ functions (symbols). The inset presents the schematic phase diagram in which a line of classical phase transition ends at QCP.

independent of a physical mechanism of the transition, predicted by the renormalization group theory for the second-order phase transitions, (iii) at analyzing if these behaviors are characteristic of the transitions having a quantum character, i.e., influenced by QFs, and (iv) at considering possible mechanisms of the transition found.

It should be noted that $RT_3(BO_3)_4$ crystals with $R =$ Y, or a rare-earth ion, and $T =$ Al, Ga, Cr, or Fe, attract attention because they are suitable for laser applications (e.g., aluminoborates doped with Nd are used in self-doubling frequency lasers), show large magnetoelectric effect [10,11] and different magnetocrystalline anisotropy for various R ions [12]. Thus, deep knowledge of their properties over a wide temperature range is highly desirable.

II. EXPERIMENT

$RAl_3(BO_3)_4$ compounds with $R =$ Y, Sm–Yb crystallize in a trigonal structure (space-group no. 155, $R32$), Fig. 1(a), with three formula units in the trigonal unit cell [13]. Magnetic R^{3+} ions are located inside the deformed trigonal prisms formed by six O^{2-} ions. The R-O_6 prisms, separated along the c axis by B-O_3 triangles, form chains along the threefold c axis. Between the neighboring chains, other B-O_3 triangles and oxygen octahedra containing Al^{3+} ions are located.

For the 0.514(2)-mg plate, cut perpendicularly to the c axis from the $TbAl_3(BO_3)_4$ single crystal grown by using the flux method [14,15], specific heat, and magnetization were measured as a function of T and magnetic field applied along $\mathbf{B}_\parallel$ and perpendicularly $\mathbf{B}_\perp$ to the c axis.

C_B was measured by means of the relaxation method by using the Quantum Design Physical Property Measurement System (PPMS), equipped with the Dilution Refrigerator and Heat Capacity Options. To gather the data for estimating the lattice specific heat C_l, the measurements were performed from 50 mK to 300 K for $B = 0$. Since these studies showed that a certain unknown phase transition appears at 0.68 K, the detailed C_B studies were performed for the 50 mK–4 K range for $B = 0$ and for several $B_\parallel$ and $B_\perp$ values up to 3 T. It was verified that for both zero and nonzero B, no C_B singularities appear above 4 K. Near the discovered transition, C_B was measured each 2 mK, whereas outside this region, over the range of 50 mK–1 K, each ~10 mK.

By using the Quantum Design MPMS-XL superconducting quantum interference device magnetometer equipped with the Helium 3 option, $M(T)$ functions were measured for several $B_\parallel$ values (0.01, 0.1, 0.2, 0.25, and 0.35 T) for 0.5 K $\leqslant T \leqslant 1$ K. At $T = 0.5$ K, the $M(B)$ function was measured for $B_\parallel$ and $B_\perp$.
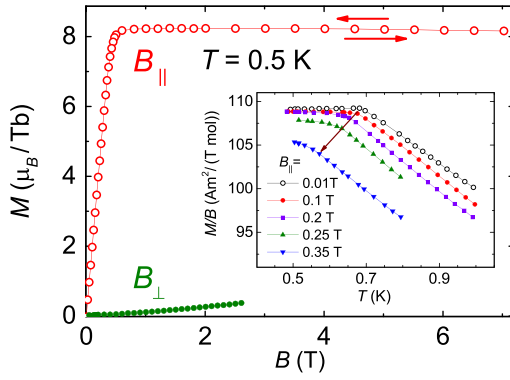
FIG. 2. Magnetization of the $TbAl_3(BO_3)_4$ single crystal (not corrected for demagnetizing effects). Main panel, M versus $B_\parallel$ and $B_\perp$ at $T = 0.5$ K. The inset, M/B versus T for $B_\parallel = 0.01$, 0.1, 0.2, 0.25, and 0.35 T. The arrow indicates evolution of the transition temperature with an increase in $B_\parallel$.

III. RESULTS

Results of the C_B and M measurements are presented in Figs. 1 and 2.

In order to extract the most interesting for the present studies, magnetic or nonphonon contribution C_m to C_B, we modeled $C_l(T)$ with the expression,

$$C_l(T) = \left[3 n_D \left(\frac{T}{\theta_D} \right)^3 \int_0^{\theta_D/T} \frac{x^4 e^x}{(e^x - 1)^2} dx \right.$$
$$\left. + \sum_{i=1}^{n_O} n_i \left(\frac{\theta_i}{T} \right)^2 \frac{e^{\theta_i/T}}{(e^{\theta_i/T} - 1)^2} \right] \frac{k_B N_A}{(1 - \alpha T)}, \quad (2)$$

which mimics the contribution related to acoustic and some optical phonons in frames of the Debye model (the first term in the parentheses), the contribution related to remaining optical phonons in frames of the Einstein model (the second term in the parentheses), and takes into account the effect of thermal lattice expansion by the method proposed in Ref. [16] (the $1 - \alpha T$ denominator). It was used successfully for describing the lattice specific heat of many materials, e.g., of layered cobaltites [17] and olivines [18]. We fitted (2) to the data measured for $TbAl_3(BO_3)_4$ in $B = 0$ above 15 K because as Fig. 1(b) illustrates, for $T > 15$ K, all other than C_l contributions can be neglected. The best description of $C_l(T)$ was achieved by taking the following values of the fitted parameters: $\alpha = 0.00129$ K^{-1}, $n_D = 3$, $\theta_D = 465$ K, $n_O = 6$, and, for $i = 1, 2, \ldots, 6$, respectively, $n_i = 1, 2, 3, 2, 6$, and 6, and $\theta_i = 105, 160, 302, 462, 496$, and 565 K. The θ_i values represent energies of the lowest optical branches, expressed in temperature units. They agree qualitatively with the energies of optical phonons corresponding to translations of the R^{3+} ions as well as to translations and librations of the BO_3 complexes, given in Ref. [19].

C_m determined as the difference between the measured $C_B(T)$ and the estimated $C_l(T)$ is presented in Figs. 1(c) and 1(d). At low T for $B_\parallel < 0.475$ T, the $C_m(T, B_\parallel = $ const$)$ functions show: (i) a λ-shaped anomaly [at $T = 680(2)$ mK for $B = 0$], which decreases and shifts towards lower temperatures with increasing $B_\parallel$, (ii) a practically field-independent

minimum $C_m = 1.10(5)$ J/(mol K) at $T_m = 290(1)$ mK, and (iii) upturn with decreasing T below T_m. The temperature range in which this upturn could be studied in our apparatus was limited by a strong increase in the heat relaxation time with lowering T, and as a result, no reliable specific heat values could be measured below 160 mK for $B = 0$ and 200 mK for $B_\parallel = 0.4$ T. For $B_\parallel > 0.475$ T, Figs. 1(c) and 1(e), a sudden disappearance of the λ anomaly and of the minimum at T_m are observed, and C_m decreases with decreasing T monotonically, down to unmeasurable values. Thus, the lowest experimental points were measured at $\sim$390 mK for $B_\parallel = 0.7$ T and at $\sim$640 mK for $B_\parallel = 1$ T.

IV. ANALYSIS

The asymmetric λ shape of the anomalies found in the $C_m(T, B = $ const$)$ functions, their rather large width, and lack of thermal hysteresis of their appearance on heating and on cooling the sample allow to assume that they are related to a second-order phase transition. Of course, the lack of hysteresis is the necessary but not sufficient condition only and the two former arguments are rather heuristic. Thus, a more detailed analysis whether the specific heat as a function of temperature and magnetic field shows universal critical behaviors characteristic of the second-order transitions, predicted by the renormalization group theory and independent of a physical mechanism of the transition, is necessary to identify the order of the found transition unequivocally. Such analysis was performed and will be presented below.

The specific heat data, Fig. 1, the magnetization curves presented in Fig. 2, as well as high sensitivity of the phase-transition temperature to $B_\parallel$ suggest the transition to be related to ordering of magnetic moments of the Tb^{3+} ions, being the only magnetic ions in the system. The shape of the magnetization curve for $B_\parallel$, presented in Fig. 2, and the measured saturation magnetization of $TbAl_3(BO_3)_4$, $8.2\mu_B$/Tb, being close to the magnetic moment of the free Tb^{3+} ($9\mu_B$) ion, suggest that we deal with the ferromagnetic ordering. However, if it were the classical transition between the paramagnetic and ferromagnetic phases, induced by thermal fluctuations, $\mathbf{B}_\parallel$ should smear it and shift it towards higher T. Actually, we observe the opposite counterintuitive effect. The λ anomaly remains sharp and shifts towards lower T with increase in $B_\parallel$, i.e., it behaves in a way characteristic of antiferromagnets. Thus, we suppose that the transition found has a quantum character, i.e., it is dominated by QFs, which destroy the long-range ferromagnetic order. In other words, we deal with one of the two model cases considered in the physics of quantum transitions [1,20], shown schematically in the inset to Fig. 1(f) in which the line of classical transitions ends at QCP. Below, we analyze, if other characteristics of the transition support this idea. However, the possibility that Tb-Tb exchange interactions are not the main driving force leading to the ferromagnetic order, but some other mechanism is responsible for the transition evolving to QCP and the ordering of Tb^{3+} moments is a side effect only, cannot be excluded a priori. An ordering of electric quadrupolar moments of the Tb-O_6 complexes, cooperative-Jahn-Teller effect, or a more complex multipolar ordering [21,22] could be indicated as such possible mechanisms.

To interpret the presence of the minimum at T_m and of the upturn of $C_m(T, B = \text{const})$ on lowering T below T_m for $B_\parallel < 0.475$ T, we assumed C_m to be the sum of the critical contribution C_{cr}, related to the phase transition, and the nuclear specific heat C_N, related to excitations of magnetic Tb nuclei. C_N grows on lowering temperature and becomes a dominating contribution to the measured specific heat C_B below T_m. Following the analysis presented in Ref. [23], we verified that for $TbAl_3(BO_3)_4$, the nuclear quadrupole interaction can be neglected. Then, the Hamiltonian of the nucleus can be presented in the form $\hat{H} = a\hat{I}_z$, where $\hat{I}_z$ is the operator of the z component of the nuclear spin, and a is the coefficient of the interaction between the nuclear magnetic moment and the hyperfine field B_{hyp}. For Tb^{3+}, $I = 3/2$, and the nuclear magnetic moment is equal to $1.994\mu_N$ (μ_N is the nuclear magneton). Thus, expressing energy in temperature units, we obtain the following formula for the nuclear contribution to the molar specific heat of $TbAl_3(BO_3)_4$:

$$C_N(T) = \frac{R}{T^2} \frac{a^2[\cosh(2a/T) + 4\cosh(a/T) + 5]}{2[\cosh(3a/2T) + \cosh(a/2T)]^2}, \quad (3)$$

where $|a| = B_{hyp} 1.994\mu_N 2/(3k_B)$ and R denotes the gas constant. In the further analysis, we treated the hyperfine field B_{hyp} as the fitted parameter.

According to Refs. [3,4], in the vicinity of a quantum second-order transition, the scaling relation for the critical contribution to free energy F_{cr} has a form

$$F_{cr}(T) = -R\rho_0 |r|^{\nu(d+z)} \widetilde{f}\left(\frac{T}{T_0 |r|^{\nu z}}\right), \quad (4)$$

where $\widetilde{f}(x)$ is a universal scaling function, d is dimension of the considered system, $r = (B - B_c)/B_c$ is the control parameter describing the distance from the QCP at $T = 0$ and $B = B_c$, ρ_0 and T_0 are nonuniversal parameters, ν is the exponent of the critical behavior of the correlation length near QCP, $\xi \sim |r|^{-\nu}$, and z is the "dynamical critical exponent" describing the correlation length $\xi_\tau \sim \xi^z$ along the direction of "imaginary time" $\tau = i\hbar/(k_B T)$. For $B = B_c$, for the system evolving along the trajectory denoted as b in the schematic phase diagram in the inset to Fig. 1(f), the free energy is a regular function of T that can be expanded into the Taylor series. However, at $B < B_c$, for the system evolving along the a trajectory and meeting on its way the classical phase transition, the free energy shows a more peculiar behavior. In the limit of $T \to 0$ and $r \neq 0$, $\widetilde{f}(x)$ can be approximated by the formula $\widetilde{f}(x \to 0) = \widetilde{f}(0) + cx^{y_0+1}$, where y_0 is a positive exponent. Thus, differentiating (4) with respect to T, one obtains the entropy, and next, by differentiating it with respect to T and B, one obtains the following formulas for the critical specific heat C_{cr} and Γ, valid for the area below the line of classical phase transitions, denoted in the inset to Fig. 1(f) as the ordered phase:

$$C_{cr}(T \to 0, B) = T\frac{\partial S}{\partial T} = C_1(B)T^{y_0}, \quad (5)$$

$$C_1(B) = R\frac{\rho_0 c y_0(y_0 + 1)}{T_0^{y_0+1}}\left|\frac{B - B_c}{B_c}\right|^{\nu(d-y_0 z)}, $$

$$\Gamma(T \to 0, B) = -\frac{G_B}{B - B_c}, \quad \text{with } G_B = \frac{\nu(d - y_o z)}{y_0}, \quad (6)$$

By assuming C_m to be the sum of C_N and C_{cr} (5),

$$C_m(T, B = \text{const}) = C_N(T) + C_1(B)T^{y_0}, \quad (7)$$

and treating B_{hyp}, C_1, and y_0 as fitted parameters, a good description of the experimental $C_m(T)$ dependence for $B = 0$ [thick solid red line in Fig. 1(d)] was achieved. The best fit value $B_{hyp} = 227.7(1)$ T seems to be reasonable because for the magnetically ordered terbium metal [24] and alloys [25], the values of 360 ± 40 T were reported. As Fig. 1(c) shows, $B_\parallel < 0.4$ T has no influence on C_N because for these $B_\parallel$ values, all $C_m(T)$ curves overlap below T_m. Thus, it was assumed that B_{hyp} remains constant for $B_\parallel < 0.4$ T, then for larger $B_\parallel$, it falls down due to destruction of the long-range order of Tb^{3+} magnetic moments, and for $B_\parallel > 0.55$ T, C_N becomes unmeasurably small. We found that the sinusoidal anomaly of the experimental $C_m(T, B = 0)$ curve, visible in Fig. 1(d) between 0.25 and 0.35 K, is not a physical effect because it is the same for all $B_\parallel \leqslant 0.475$ T and appears also for samples of other composition. Thus, it was interpreted as an apparatus effect and eliminated from the experimental $C_m(T, B_\parallel = \text{const})$ curves for $B_\parallel \leqslant 0.475$ T by subtracting from them the difference between the experimental and theoretical [red solid line in Fig. 1(d)] $C_m(T, B = 0)$ curves for the range $242 \leqslant T \leqslant 479$ mK. The corrected functions (for $B_\parallel \leqslant 0.4$ T) denoted as C_{mc} are plotted in Fig. 1(e) together with the curves (7) fitted to them (red solid lines) by taking $B_{hyp} = 227.7(1)$ T and fitting C_1 and y_0. Next, assuming the λ maxima of the $C_m(T, B)$ functions to correspond to the phase-transition temperature, we constructed the $B_\parallel - T$ phase diagram, Fig. 1(f). We found that the power function: 0.681 K $- a_1 B^{a_2}$ with $a_1 = 2.65(5)$ K, $a_2 = 2.65(5)$, and B given in teslas describes the experimental phase-transition line very well and gives the hypothetical quantum critical field value $B_c = 0.600(1)$ T. With this B_c value, the phase-transition line for 0.35 T $\leqslant B_\parallel \leqslant B_c$ can be described by the typical critical dependence: $d_1(B_c - B_\parallel)^{d_2}$ with $d_1 = 1.75(3)$ K, $d_2 = 0.85(1)$, and $B_\parallel$ given in teslas. Using this B_c in the definition of r, we obtained that the $0 \leqslant B_\parallel \leqslant 0.475$ T values correspond to $1 \geqslant r \geqslant 0.21$. This result is essential because usually one assumes the critical behavior to appear for $r < 10^{-3}$, thus, the behaviors observed in our experiments should be extrapolated to smaller r values to get actual critical behaviors of the studied system.

Plots of the found y_0 and C_1 values as a function of $B_\parallel$ [the inset to Fig. 1(b)] can be approximated by, drawn with the black solid lines, the field-independent $y_0 = 2.71(7)$ value and the $C_1(B_\parallel) = c_1(B_c - B_\parallel)^{c_2}$ function with $c_1 = 45.7$ J/(mol K), $c_2 = 0.35$, and $B_\parallel$ given in teslas. Comparing the $C_1(B_\parallel)$ function and (6) we get

$$z = (d - c_2/\nu)/y_0. \quad (8)$$

The $\Gamma(T)$ functions for different $B_\parallel$s were estimated by substituting into (1) the $C_{mc}(T, B_\parallel)$ functions determined and the $(\partial M/\partial T)_{B_\parallel}$ derivatives, approximated by the difference quotients, calculated basing on the measured $M(T, B_\parallel)$ functions, Fig. 2. For $B_\parallel = 0.3$ T for which M was not measured, $\partial M/\partial T$ was estimated as the average of the values calculated for $B_\parallel = 0.25$ and 0.35 T. The results are shown in Fig. 3(b). In principle, having $C_{mc}(T)$ for different $B_\parallel$s, it was possible to calculate the entropies $S(T, B_\parallel = \text{const}) = \int C_{mc}/T \, dT$ and
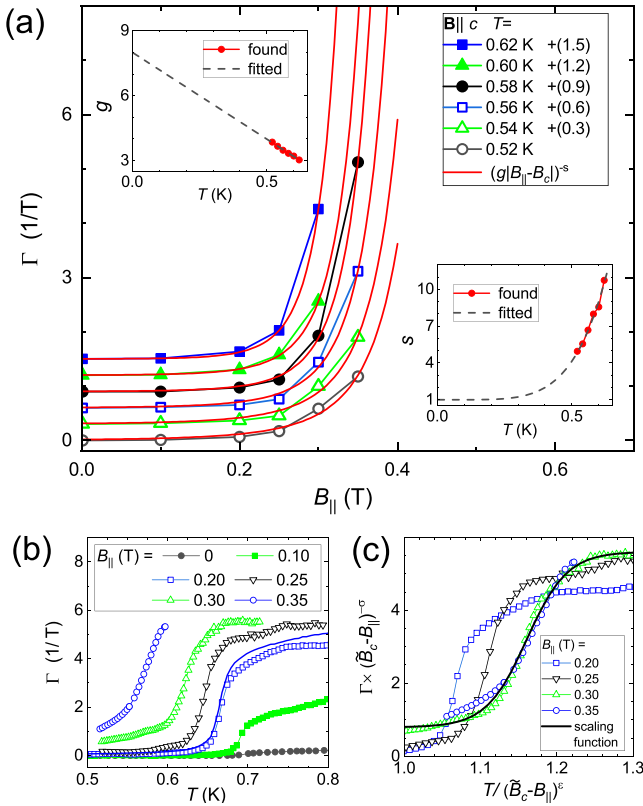
FIG. 3. The Grüneisen ratio Γ. (a) Γ values as a function of $B_\parallel$, symbols, and the theoretical $g|B - B_c|^{-s}$ functions fitted to them, solid red lines, for several T values. Curves for different Ts are shifted along the Γ axis by the values given in the legend in parentheses. The insets, g and s parameters as a function of T. (b) $\Gamma(T)$ for several $B_\parallel$s, symbols. The blue solid line is the $\Gamma(T, B_\parallel = 0.2\ \text{T})$ function calculated based on the $C_{mc}(T)$ curves. (c) Scaling behavior. $\Gamma(\widetilde{B}_c - B_\parallel)^{-\sigma}$ as a function of $T/(\widetilde{B}_c - B_\parallel)^\epsilon$ for $\epsilon = 0.48(4)$, $\sigma = 0$, and $\widetilde{B}_c = 0.57(3)$ T for several $B_\parallel$s. The black solid line is the approximation of the scaling function: $\Phi(x) = 3.2 + 2.4 \tanh[19(x - 1.161)]$. The curves for $B_\parallel \geqslant 0.3$ T overlap for the arguments 1.132–1.221.

$\partial S / \partial B$. However, $C_B(T)$ was measured for a few $B_\parallel$ values only and, hence, the approximation of $\partial S / \partial B$ with the difference quotients was rough. Thus, this method of determining Γ was less accurate, and only one of such determined functions for $B_\parallel = 0.2$ T is shown in Fig. 3(b) as an example. The $\Gamma(T)$ functions were converted into $\Gamma(B_\parallel)$ functions, shown in Fig. 3(a) for several fixed T values. It was found that they cannot be described by the formula (6), but they can be approximated by formula,

$$\Gamma(B_\parallel, T = \text{const}) = [g(B_c - B_\parallel)]^{-s}. \tag{9}$$

The functions (9) fitted to the experimental data for different Ts are plotted in Fig. 3(a) with red solid lines, and the g and s parameters of the best-fit lines are plotted as a function of T in the insets to Fig. 3(a). As the dashed lines show: (i) the $s(T)$ function can be approximated by $s(T) = 1 + 111T^{5.1}$ for T given in kelvins, which, when extrapolated to $T < 0.2$ K, gives the $s(T) \approx 1$ value, consistent with the theoretical prediction (6), and (ii) $g(T)$ can be approximated by the straight

line $g(T) = 8 - 8T$ for T given in kelvins, which allows to assume the parameter G_B appearing in (6) to be $G_B \approx 1/g(0) = 0.125(2)$. Thus, based on (8) and (6), using the determined y_0, c_2, and $g(0)$ parameters, and taking into account experimental uncertainties, we obtain $1/g(0) = c_2/y_0 \approx 0.126(3)$ and

$$z = d/y_0 - 1/[\nu g(0)] = d/y_0 - 0.126/\nu. \tag{10}$$

By assuming that the we deal with the three-dimensional (3D) magnetic system ($d = 3$) and that ν takes a value between $1/2$ (found in the molecular field model) and 0.715 (found for the 3D Heisenberg model), we find the dynamical critical exponent of the studied system to be $0.82 \leqslant z \leqslant 0.96$.

Seeking for a based on scaling argument for the quantum character of the transition analyzed, we relied on the observation [26], that for some systems, near QCP with the critical field $\widetilde{B}_c$, Γ scales with $T(\widetilde{B}_c - B)^{-\epsilon}$ with a constant ϵ. Thus, we assumed that at quantum criticality, Γ is a generalized homogeneous function relative $\widetilde{B}_c - B$, which fulfills the relation $\Gamma(T, \widetilde{B}_c - B) \sim (\widetilde{B}_c - B)^\sigma \Phi[T(\widetilde{B}_c - B)^{-\epsilon}]$ with a constant σ and Φ being a scaling function. If the scaling occurs, it should be possible to find such $\widetilde{B}_c$, σ, and ϵ that in the critical region, the plots $\Gamma(\widetilde{B}_c - B)^{-\sigma}$ versus $T(\widetilde{B}_c - B)^{-\epsilon}$ for different B values collapse onto a single curve Φ. As Fig. 3(c) shows, such a collapse of the curves for $B_\parallel = 0.30$ and 0.35 T was achieved by taking $\widetilde{B}_c = 0.57(3)$ T, $\epsilon = 0.48(4)$, and $\sigma = (437 \pm 2) \, 10^{-6} \approx 0$. Practically zero σ value confirms the Γ scaling assumed in Ref. [26]. The data sets for $B_\parallel < 0.3$ T do not follow the scaling curve, which suggests that these field values are below the quantum critical region. The $\widetilde{B}_c = 0.57(3)$ T value found from scaling is slightly smaller than that found from extrapolation of the phase-transition line shown in Fig. 1(f), which suggests that the real QCP is located between 0.57 an 0.6 T.

In order to study influence of the magnetic field directed perpendicularly to the easy magnetization c-axis ($B_\perp$) on the observed magnetic phase transition, temperature dependence of the specific heat C_B was measured for several fixed values of the field applied intentionally perpendicularly to the c axis. Next, the nonphonon contribution to it C_m, was determined by subtracting C_l from the measured C_B, i.e., in the same way as for the case of $B_\parallel$. As Fig. 4 shows, $B_\perp$ applied intentionally perpendicularly to the c axis, influences the transition weaker than $B_\parallel$ does and shifts the transition point, identified as the C_m maximum, towards lower temperatures. However, it must be taken into account that in the PPMS system used, the calorimeter is suspended by eight thin wires and in $B_\perp$ a torque is applied to the sample. As the result, the sample tilts and the c axis is no longer perpendicular to the applied field. Thus, we analyzed whether the shift of the transition can be attributed to tilting of the sample only, i.e., we assumed that the perpendicular to the c axis component of the field has no influence on the transition, and only the parallel component, appearing in the result of tilting, affects the transition. Then, based on the phase diagram constructed for $B_\parallel$, presented in Fig. 1(f), we determined what $B_\parallel$, i.e., what tilting angle, would be necessary to cause the observed shift in the transition. As indicated in the legend of Fig. 4, the expected tilt angles are quite probable and grow monotonically up to 20°.
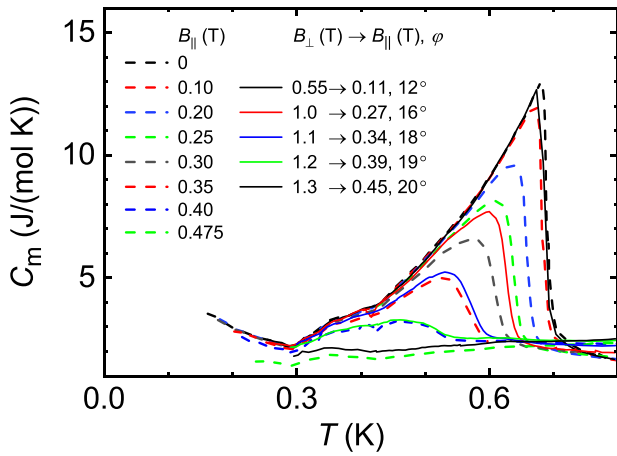
FIG. 4. $C_m(T)$ functions for several fixed $B_\parallel$ (dashed curves) and applied intentionally perpendicularly to the c axis $B_\perp$ (solid lines) values. In the legend, the expected sample tilting angles (calculated under assumption that only the $B_\parallel$ component influences the transition point) as well as corresponding to them $B_\parallel$ components are given.

Thus, we find the assumption, that the transition is insensitive to $B_\perp$ to be well grounded.

V. CONCLUSIONS

Based on the detailed studies of specific heat C_B and magnetization M below 1 K, we found a magnetic phase transition in TbAl$_3$(BO$_3$)$_4$, which shifts to lower temperatures with an increase in magnetic field $\mathbf{B}_\parallel$, parallel to the easy magnetization axis. Determined behaviors of both C_B and the Grüneisen ratio Γ as a function of T (especially scaling of the latter for $B_\parallel \geqslant 0.30$ T) as well as dependence of Γ on $B_\parallel$ are characteristic of systems in which the classical phase-transition line is influenced by QFs and ends at QCP. Vanishing of the nuclear specific heat for $B_\parallel > 0.475$ T confirms that $B_\parallel$

destroys the long-range magnetic order. The value of the dynamical critical exponent z was assessed to $0.82 \leqslant z \leqslant 0.96$. However, a physical nature of the transition is not clear. The interpretation that this is the transition to the ferromagnetic order of Tb^{3+} magnetic moments is the most natural, intuitive, and supported by the studies of M. However, such a classical transition should be smeared and shifted to higher T by $B_\parallel$, whereas we observe the opposite effect. We attribute this to QFs, which dominate the behavior of the system and destroy the long-range order, i.e., we suppose the transition to have quantum character. On the other hand, the behavior observed would be consistent with the behavior of the transition to an antiferromagnetic phase, but the studies of M, e.g., lack of a metamagnetic transition, linear dependence of M on $B_\parallel$, and reaching saturation magnetization nearly equal to the magnetic moment of free Tb^{3+} ions in small $B_\parallel \sim 0.7$ T, contradict this interpretation. Also the possibility, that the transition is not a magnetic one but related to any other kind of ordering, e.g., a complex multipolar ordering, and the ordering of the Tb^{3+} moments is a side effect only, related to the strong magnetoelectric effect present in these materials, cannot be ruled out. Generally, a physical mechanism proposed must predict not only the decrease in the transition point with an increase in $B_\parallel$, but also the other unusual behaviors, such as $C_{\mathrm{cr}} \sim T^{y_0}$ and divergence of Γ, found in the present studies. To elucidate the physical mechanism responsible for the transition, detailed neutron-diffraction studies are necessary but due to the low transition temperature and the presence of boron, very highly absorbing neutrons, such studies would be very difficult, although possible [11].

[1] S. Sachdev, *Quantum Phase Transitions* (Cambridge University Press, Cambridge, UK, 2011).

[2] P. Gegenwart, Q. Si, and F. Steglich, Quantum criticality in heavy-fermion metals, Nat. Phys. **4**, 186 (2008).

[3] L. Zhu, M. Garst, A. Rosch, and Q. Si, Universally Diverging Grüneisen Parameter and the Magnetocaloric Effect Close to Quantum Critical Points, Phys. Rev. Lett. **91**, 066404 (2003).

[4] M. Garst and A. Rosch, Sign change of the Grüneisen parameter and magnetocaloric effect near quantum critical points, Phys. Rev. B **72**, 205129 (2005).

[5] H. Kadowaki, H. Takatsu, and M. Wakita, Dimensional change of the quadrupole order in pseudospin-$\frac{1}{2}$ pyrochlore magnets under magnetic field in the [111] direction, Phys. Rev. B **98**, 144410 (2018).

[6] H. Ryll, K. Kiefer, C. Rüegg, S. Ward, K. W. Krämer, D. Biner, P. Bouillot, E. Coira, T. Giamarchi, and C. Kollath, Magnetic entropy landscape and Grüneisen parameter of a quantum spin ladder, Phys. Rev. B **89**, 144416 (2014).

[7] L. Gálisová and J. Strečka, Magnetic Grüneisen parameter and magnetocaloric properties of a coupled spin-electron double-tetrahedral chain, Phys. Lett. A **379**, 2474 (2015).

[8] B. Wolf, Y. Tsui, D. Jaiswal-Nagar, U. Tutsch, A. Honecker, K. Removic-Langer, G. Hofmann, A. Prokofiev, W. Assmus, G. Donath, and M. Lang, Magnetocaloric effect and magnetic cooling near a field-induced quantum-critical point, Proc. Natl. Acad. Sci. USA **108**, 6862 (2011).

[9] V. A. Bedarev, M. I. Paschenko, M. I. Kobets, K. G. Dergachev, E. N. Khatsko, S. L. Gnatchenko, A. A. Zvyagin, T. Zajarniuk, A. Szewczyk, M. U. Gutowska, L. N. Bezmaternykh, and V. L. Temerov, Low-temperature magnetic phase transition in aluminum borate TbAl$_3$(BO$_3$)$_4$, Low Temp. Phys. **41**, 534 (2015).

[10] K.-C. Liang, R. P. Chaudhury, B. Lorenz, Y. Y. Sun, L. N. Bezmaternykh, V. L. Temerov, and C. W. Chu, Giant magnetoelectric effect in HoAl$_3$(BO$_3$)$_4$, Phys. Rev. B **83**, 180417(R) (2011).

[11] H. Zhang, S. Liu, C. S. Nelson, L. N. Bezmaternykh, Y.-S. Chen, S. G. Wang, R. P. S. M. Lobo, K. Page, M. Matsuda,

D. M. Pajerowski, T. J. Williams, and T. A. Tyson, Structural features associated with multiferroic behavior in the $RX_3(BO_3)_4$ system, J. Phys.: Condens. Matter **31**, 505704 (2019).

[12] K.-C. Liang, R. P. Chaudhury, B. Lorenz, Y. Y. Sun, L. N. Bezmaternykh, I. A. Gudim, V. L. Temerov, and C. W. Chu, Magnetoelectricity in the system RAl$_3$(BO$_3$)$_4$ ($R =$ Tb, Ho, Er, Tm), J. Phys.: Conf. Ser. **400**, 032046 (2012).

[13] N. Leonyuk and L. Leonyuk, Growth and characterization of $RM_3(BO_3)_4$, Prog. Cryst. Growth Charact. Mater. **31**, 179 (1995).

[14] E. V. Eremin, N. V. Volkov, V. L. Temerov, and I. A. Gudim, Specific features of magnetic properties of Tb$_{1-x}$Ho$_x$Al$_3$(BO$_3$)$_4$ aluminoborates, Phys. Solid State **58**, 660 (2016).

[15] I. A. Gudim, E. V. Eremin, and V. L. Temerov, Flux growth and spin reorientation in trigonal Nd$_{1-x}$Dy$_x$Fe$_3$(BO$_3$)$_4$ single crystals, J. Cryst. Growth **312**, 2427 (2010).

[16] C. A. Martin, Simple treatment of anharmonic effects on the specific heat, J. Phys.: Condens. Matter **3**, 5967 (1991).

[17] J. Wieckowski, M. U. Gutowska, A. Szewczyk, S. Lewinska, K. Conder, E. Pomjakushina, V. P. Gnezdilov, and S. L. Gnatchenko, Thermal properties of layered cobaltites RBaCo$_2$O$_{5.5}$ ($R =$ Y, Gd, and Tb), Phys. Rev. B **86**, 054404 (2012).

[18] S. Lewińska, A. Szewczyk, M. U. Gutowska, J. Wieckowski, R. Puzniak, R. Diduszko, A. Reszka, B. J. Kowalski, Y. Kharchenko, and J. Molenda, Magnetic susceptibility and phase transitions in LiNiPO$_4$, Phys. Rev. B **99**, 214440 (2019).

[19] E. A. Dobretsova, E. Y. Borovikova, K. N. Boldyrev, V. S. Kurazhkovskaya, and N. I. Leonyuk, IR spectroscopy of rare-earth aluminum borates RAl$_3$(BO$_3$)$_4$ ($R =$ Y, Pr − Yb), Opt. Spectrosc. **116**, 77 (2014).

[20] M. Vojta, Quantum phase transitions, Rep. Prog. Phys. **66**, 2069 (2003).

[21] P. Santini, S. Carretta, G. Amoretti, R. Caciuffo, N. Magnani, and G. H. Lander, Multipolar interactions in f-electron systems: The paradigm of actinide dioxides, Rev. Mod. Phys. **81**, 807 (2009).

[22] J. Sivardière and M. Blume, Dipolar and quadrupolar ordering in $s = 3/2$ Ising systems, Phys. Rev. B **5**, 1126 (1972).

[23] O. V. Lounasmaa and P. R. Roach, Specific heat of terbium metal between 0.37 and 4.2 K, Phys. Rev. **128**, 622 (1962).

[24] E. C. Heltemes and C. A. Swenson, Nuclear contribution to the heat capacity of terbium metal, J. Chem. Phys. **35**, 1264 (1961).

[25] R. Vijayaraghavan, K. Shimizu, J. Itoh, A. K. Grover, and L. C. Gupta, Hyperfine field studies in magnetically ordered samarium and terbium alloys, J. Phys. Soc. Jpn. **43**, 1854 (1977).

[26] P. Gegenwart, Classification of materials with divergent magnetic Grüneisen parameter, Philos. Mag. **97**, 3415 (2017).